Chemistry & Biology
Resource

Knowledge-Based Design of a Biosensor to Quantify Localized ERK Activation in Living Cells

Lutz Kummer,[1] Chia-Wen Hsu,[2] Onur Dagliyan,[3] Christopher MacNevin,[2] Melanie Kaufholz,[4] Bastian Zimmermann,[4] Nikolay V. Dokholyan,[3] Klaus M. Hahn,[2] and Andreas Plückthun[1,*]
[1]Department of Biochemistry, University of Zurich, Winterthurerstrasse 190, 8057 Zurich, Switzerland
[2]Department of Pharmacology
[3]Department of Biochemistry and Biophysics
School of Medicine, University of North Carolina at Chapel Hill, Chapel Hill, NC 27599, USA
[4]Biaffin GmbH & Co KG, Heinrich-Plett-Strasse 40, 34132 Kassel, Germany
*Correspondence: plueckthun@bioc.uzh.ch
http://dx.doi.org/10.1016/j.chembiol.2013.04.016

SUMMARY

Investigation of protein activation in living cells is fundamental to understanding how proteins are influenced by the full complement of upstream regulators they experience. Here, we describe the generation of a biosensor based on the DARPin binding scaffold suited for intracellular applications. Combining library selection and knowledge-based design, we created an ERK activity biosensor by derivatizing a DARPin specific for phosphorylated ERK with a solvatochromatic merocyanine dye, whose fluorescence increases upon pERK binding. The biosensor specifically responded to pERK2, recognized by its conformation, but not to ERK2 or other closely related mitogen-activated kinases tested. Activated endogenous ERK was visualized in mouse embryo fibroblasts, revealing greater activation in the nucleus, perinuclear regions, and especially the nucleoli. The DARPin-based biosensor will serve as a useful tool for studying biological functions of ERK in vitro and in vivo.

INTRODUCTION

Traditional methods for studying signal transduction cascades are based on biochemical methods, which have provided valuable insight into the function and regulation of signaling pathways. However, these methods can only probe interactions with specific proteins; they do not report activation of proteins in their native environment within living cells, and ignore transport processes and diffusion. Fluorescent biosensors based on affinity probes have been developed as an alternative approach to quantifying protein activity in vivo (Gulyani et al., 2011; Nalbant et al., 2004; MacNevin et al., 2013). At present, specific binding probes are often proteins, in most cases antibodies. Although antibodies and their engineered derivatives provide great specificity, affinity, and variability, they have several intrinsic limitations. Most importantly, their reliance on disulfide bonds hampers their use in the reducing cytoplasmic milieu when expressed as intrabodies.

These problems led to the development of alternative families of target-binding proteins based on stable polypeptide scaffolds devoid of cysteine residues and disulfide bonds, thus ideally suited for applications in reducing cellular environments (Binz et al., 2005). As a prominent example, designed ankyrin repeat proteins (DARPins) possess remarkable biophysical properties, which are more favorable than those of antibody fragments for their use in the design of biosensors (Brient-Litzler et al., 2010). DARPins are based on domains consisting of ankyrin repeats that are present in a great number of proteins across all phyla and are involved in specific recognition between proteins (Mosavi et al., 2004). A consensus design-based approach was used to generate combinatorial libraries of DARPins by randomization of less conserved residues identified by sequence and structure analyses (Binz et al., 2003). DARPins consist of 33-amino acid-long, consecutive homologous structural modules with fixed framework and variable potential interaction residues, which stack together to form elongated protein domains (Binz et al., 2003). Specific high-affinity binders derived from DARPin libraries can be generated against virtually any protein antigen by in vitro selection (Binz et al., 2004; Boersma and Plückthun, 2011; Kawe et al., 2006; Zahnd et al., 2006) and can serve as the basis for the design of biosensors using fluorescence readouts, such as BRET (Kummer et al., 2012), or via the attachment of environmentally sensitive dyes (Brient-Litzler et al., 2010). Importantly, the defined interaction surface and the uniformity of the DARPin scaffold simplify the sensor design through knowledge-guided attachment of fluorophores, thus minimizing previously required extensive optimization steps in order to yield functional biosensors (Brient-Litzler et al., 2010; Miranda et al., 2011; Nalbant et al., 2004).

For the application presented here, we chose to detect DARPin binding to the respective target by attachment of a bright solvatochromatic fluorophore, which has emissive properties that are dependent on the solvent environment. When positioned appropriately in the binding protein, the exposure of the dye to a hydrophobic environment, which forms upon target binding, within the new protein-protein interaction interface causes a change in fluorescence intensity and/or λ_{max}. Specifically, we

Table 1. Analysis of the Interface between DARPin pE59 and pERK2

Residue	ΔASA (Å^2)[a]	ΔASA (%)[a]	ΔΔG (kcal mol^{-1})[b]	Contact[c]
Leu53	1.8	10.4	+3.24	none
Gly91	0.0	0.0	+4.42	none
Gly113	11.9	35.9	+6.74	pERK2
Ile119	6.5	47.0	+3.54	none
Asn123	33.6	41.8	+1.34	none
Gly124	0.4	0.7	+4.90	none

[a]Variation of accessible surface area between the free and pERK2-bound states of pE59.
[b]Difference in ΔG of protein folding between DARPin pE59 and pE59 cysteine mutants, calculated by ROSETTA (Leaver-Fay et al., 2011).
[c]Contacts between pE59 and pERK2 in the structure of the complex.

have previously described a set of highly fluorescent fluorophores of the merocyanine family, which have been optimized to be part of protein-based biosensors in living cells (Gulyani et al., 2011; Nalbant et al., 2004; Toutchkine et al., 2003, 2007a, 2007b). The dyes can be excited at long wavelengths (>580 nm) to avoid cell damage and diminish cellular autofluorescence. In addition, their bright fluorescence in hydrophobic environments (quantum yield 0.17–0.61, $\varepsilon > 100{,}000$) enables the use of low concentrations of biosensor for the detection of endogenous, unaltered target proteins. Both properties, brightness and long wavelength, guarantee sensitive detection and use of low concentrations that lead to minimal perturbation of cellular mechanisms. Here we used a DARPin-based biosensor to study patterns of extracellular signal-regulated kinase (ERK) activity in living cells, where sensitivity and dynamic examination are crucial to mapping ERK function without perturbing cell physiology.

ERK belongs to the family of mitogen-activated protein kinases (MAPKs), a class of serine/threonine kinases that includes the ERK, c-Jun N-terminal kinases (JNKs), and p38 subfamilies (Chen et al., 2001). MAPKs regulate several physiological processes and play a role in pathological phenomena, including inflammation, apoptotic cell death, oncogenic transformation, tumor cell invasion, and metastasis (Pearson et al., 2001). They are part of a three-tiered phospho-relay cascade consisting of a MAPK, a MAPK kinase (MAPKK), and a MAPKK kinase (MAPKKK). Members of the ERK subfamily respond to stimuli that induce cell proliferation and differentiation (Chen et al., 2001). Depending on the cell type and the primary stimuli, ERK activity spans different subcellular compartments (Chen et al., 2001). In 3T3 fibroblasts, induction of ERK activity with epidermal growth factor (EGF) leads to a significant accumulation of activated ERK in the nucleus, which is essential for morphological transformation (Cowley et al., 1994). In contrast, EGF stimulation in PC12 cells triggers cytoplasmic ERK activity only, resulting in cellular proliferation, whereas neural growth factor causes nuclear localization, which is essential for neuronal differentiation (Marshall, 1995). Because ERK is expressed to varying extents in all tissues responding to different stimuli, a biosensor that enables visualization of activation patterns in vivo would be valuable to dissect the multiple outcomes of ERK signaling. In contrast to existing ERK activity reporters (Fujioka et al., 2006; Green and Alberola-Ila, 2005; Harvey et al., 2008; Sato et al., 2007), the dye-conjugated DARPin biosensor directly targets the active ERK conformation, rather than relying on the phosphorylation of a diffusible substrate susceptible to modification by both kinases and phosphatases.

In our study, we present a biosensor based on the DARPin scaffold that responds specifically to active doubly phosphorylated ERK (pERK). By a structure-guided approach, solvatochromatic dyes were tested at different positions adjacent to the DARPin binding interface. We identified sites for which dye attachment resulted in a specific increase of fluorescence through bound pERK2. Structural modeling of the biosensor in complex with the target confirmed our design approach and revealed insights into dye activation and sensor specificity. In addition, the created biosensor reported selectively on the changing dynamics and location of ERK activity upon stimulation or inhibition of ERK signaling in living cells.

RESULTS

Design of DARPin Conjugates

The reagentless fluorescent DARPin (RFD) biosensors described here are based on DARPin pE59, which has been selected by ribosome display to bind selectively to phosphorylated ERK2 (pERK2) (Kummer et al., 2012). pE59 reliably detects pERK, but does not bind to any other closely related member of the MAPK family in either phosphorylated or nonphosphorylated form, as shown both in vitro and in cellular assays (Kummer et al., 2012). It also does not bind to the unphosphorylated form of ERK, for which a reciprocally specific binder, E40, has been developed as well (Kummer et al., 2012).

The atomic structure of pE59 in complex with pERK2 was determined (Protein Data Bank [PDB] ID code 3ZUV) (Kummer et al., 2012). This allowed us to design and construct reagentless fluorescent biosensors by a structure-guided integration of solvatochromatic fluorophores into pE59, using a similar principle as described recently (Brient-Litzler et al., 2010), but with merocyanine dyes with excitation and emission maxima at a much higher wavelength than used earlier. An ideal site for attachment of a solvent-sensitive fluorophore must satisfy two criteria. First, the coupling site should be proximal to the putative binding site and thus offer a considerable change in the environment of the dye in the free and complexed states of pE59. Second, the attached fluorophore should neither disrupt binding between pE59 and pERK2 nor change the binding specificity of the DARPin significantly. By applying these criteria, potential coupling sites for solvent-sensitive dyes of the merocyanine family (Toutchkine et al., 2003, 2007a, 2007b) were identified by calculating changes in the accessible surface area (ΔASA) between the free and bound states of pE59 (Table 1). In total, we identified six sites in DARPin pE59 that are located in the neighborhood of pERK2 in the complex but are not involved in the interaction (Figure 1; Table 1). Residues Leu53 and Ile119 were rejected, because attachment of merocyanine dyes at these two positions probably interferes with binding to pERK2, as judged by their location in the pE59-pERK2 binding interface (Figure 1). Although no change of the ASA was calculated for Gly91 upon binding of pERK2, its location appeared to be promising for a possible solvatochromatic effect on the attached fluorophore, considering the molecular size of merocyanine dyes.

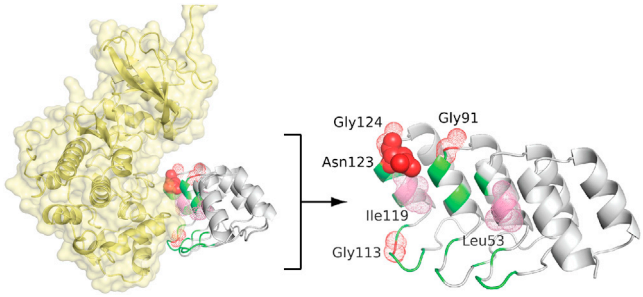

Figure 1. Sites for Dye Labeling in the Structure of DARPin pE59
Ribbon diagram of pERK2-specific DARPin pE59 (gray, based on pERK2-pE59 complex structure PDB ID code 3ZUV). Residues Gly91, Gly113, Asn123, and Gly124, which were replaced by cysteine for site-specific dye attachment, are shown in space-filling representation (red). Asn123 marks the position of dye attachment in the final pE59RFD biosensor. Residues in contact with pERK2 (yellow) in the complex structure are highlighted in green. See also Figures S1 and S2.

Production and Conjugation of DARPin-Based Sensors

The four residues Gly91, Gly113, Asn123, and Gly124 were mutated individually into cysteine by site-directed mutagenesis of the coding gene. Cysteine-containing DARPins were expressed in the cytoplasm of *Escherichia coli* and purified by immobilized metal-ion-affinity chromatography (IMAC) through their hexahistidine tag with yields comparable to wild-type pE59 (pE59-wt) (~60–80 mg/l). Calculated differences of ΔG in protein folding of pE59-wt and pE59 mutants using ROSETTA (Leaver-Fay et al., 2011) suggested a destabilizing effect of introduced cysteines at the designated positions ($\Delta\Delta G > 0$ kcal mol^{-1}) (Table 1). Thus, pE59 mutants were analyzed by size-exclusion chromatography under reducing conditions and by ELISA to prove their structural integrity and functionality. All tested DARPin mutants eluted at the same volume as pE59-wt (Figure S1 available online). Furthermore, the pE59 mutants bound pERK2 similarly to pE59-wt and retained their specificity for the doubly phosphorylated form of ERK2 (Figure S2). We conclude that the introduction of cysteines at the stated positions did not alter the favorable characteristics of pE59-wt.

In a next step, functional pE59 mutants were covalently derivatized with a diverse set of merocyanine dyes bearing cysteine-reactive iodoacetamide side chains (Toutchkine et al., 2003, 2007a, 2007b) (Figure S3). The products of the coupling reactions were separated from the free fluorophore by size-exclusion chromatography. Coupling yields were calculated from the measured protein concentration and the absorbance spectrum of the purified product. Dye:protein molar ratios were between 0.8 and 1.1 in all cases. Control reactions with pE59-wt, which has no cysteine, yielded dye:protein ratios <0.09.

Properties of DARPin Conjugates

The fluorescence response of the conjugates was assayed in the presence of ERK2 and pERK2. Three conjugates showed a substantial response: dye mero53 at position 91 (pE59-C91m53), dye mero60 at position 123 (pE59-C123m60), and dye mero87 at position 123 (pE59-C123m87) (Figure 2A). The closely related dyes mero53, mero60, and mero87 showed far stronger responses than other tested fluorophores (mero61, mero62, and mero199), but the optimal response for each set occurred at different attachment positions, probably reflecting the size and orientational preferences of the dye. The best-performing dye attachment sites were both in the C-terminal part of DARPin pE59, in the vicinity of the pE59-pERK2 interface (Kummer et al., 2012). Position 91 is located in the loop connecting α helices 1 and 2 of internal repeat module 2, directly adjacent to residues that are in contact with pERK2 and that were randomized in the original design (Figure 1). Position 123 is part of α helix 1 in the C-terminal capping repeat, following residues involved in the interaction with pERK2 (Figure 1). Of the three variants, sensor pE59-C123m87 was highly specific for pERK2 and showed promising signal brightness. In contrast, for the other two conjugates, pE59-C91m53 and -C123m60, selectivity for pERK2 over ERK2 was diminished (Figure 2A). To elucidate the difference in selectivity of conjugate variants at position 123 bearing different merocyanine dyes, we analyzed pE59-C123m variants qualitatively for pERK2 binding selectivity with ELISA (Figure S4). All tested variants showed a significant loss of affinity and selectivity for pERK2 except pE59-C123m87, the sensor with the most pronounced specificity, and to a lesser extent pE59-C123m199. Selectivity in fluorescence response toward ERK2 and pERK2 was observed for variant pE59-C123m60, whereas no significant selectivity was detected by measuring binding in ELISA experiments (Figure 2A; Figure S4), but this can be explained by the saturation of the ELISA under these conditions.

Surface plasmon resonance (SPR) measurements on a Biacore instrument were carried out with the most promising sensor variant pE59-C123m87 to quantify a possible perturbation of binding to pERK2 by the attached mero87. The dissociation constant for pE59-C123m87 was 457 nM, compared to 117 nM of native pE59-wt (Kummer et al., 2012), revealing a 4-fold decrease of affinity for the given sensor variant upon incorporation of the cysteine and the dye (Figure S5). In accordance with ELISA results (Figure S4), the pERK2 binding selectivity of the conjugate was still remarkably high (selectivity pE59-C123m87 >23), but decreased by a factor of 3 compared to pE59-wt (selectivity pE59-wt >74; Kummer et al., 2012). Due to the proven selectivity in both fluorescence activation and binding assays, pE59-C123m87 was selected for further studies, and it is referred to as pE59RFD biosensor henceforth.

To characterize the fluorescence properties of the pE59RFD biosensor, we performed titration experiments with ERK2 and pERK2 (Figure 2B). The conjugate only responded to increasing amounts of pERK2. In contrast, no significant rise in fluorescence was detected for ERK2, even at high antigen concentrations, which confirmed the sensor selectivity for the phosphorylated kinase form. As a negative control, we incorporated a cysteine at the N terminus of pE59, a region that is not involved in the interaction between pE59 and pERK2 and is therefore not expected to offer a solvatochromatic effect upon target binding. As expected, N-terminal mero87-labeled pE59 (pE59-ctrl) showed no response to ERK2 or pERK2 (Figures 2B and 2C), confirming that the detected pE59RFD response was indeed a result of our design approach. Biosensor specificity was further analyzed by fluorescence assays with purified active and inactive forms of the MAPK ERK2, JNK1α1, JNK2α1, and p38α. The different MAPK family members have marked sequence and structure homologies, with a sequence identity of >40% over the highly conserved catalytic core. In agreement with the

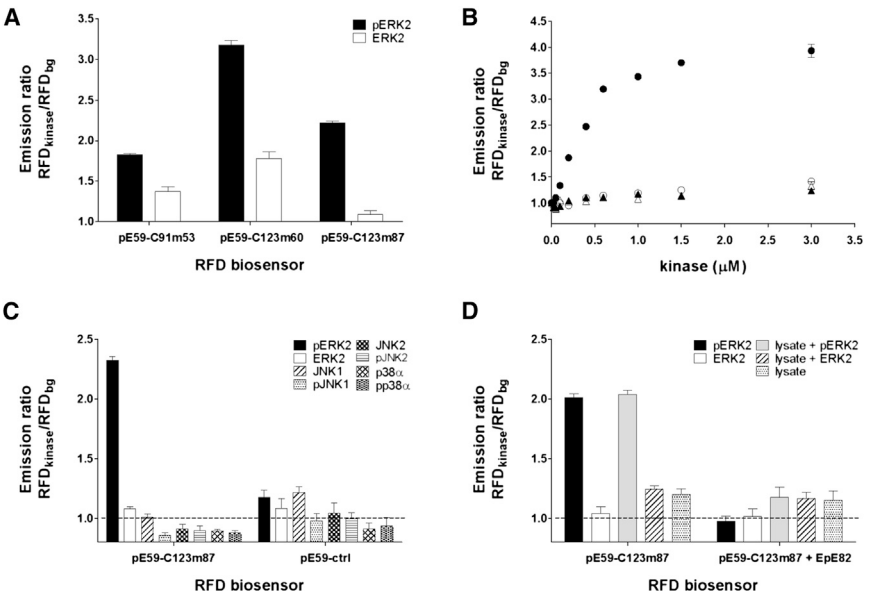

Figure 2. Characterization of RFD Biosensor Variants

Sensor responses are shown as ratiometric fluorescence emission of measurements with (RFD_{kinase}) or without (RFD_{bg}) kinase present. All experiments were performed in triplicate; error bars reflect the standard deviation.

(A) Ratiometric sensor response (RFD_{kinase}:RFD_{bg}) of three DARPin-mero conjugates when incubated with unphosphorylated or phosphorylated ERK2 (pERK2).

(B) Titration of the sensor variant pE59-C123m87 and pE59-ctrl with increasing concentrations of pERK2 and ERK2. For the control sensor, the dye was attached to the N terminus of DARPin pE59, which is not involved in the interaction with pERK2. Closed circles, sensor/pERK2; open circles, sensor/ERK2; closed triangles, pE59-ctrl/pERK2; open triangles, pE59-ctrl/ERK2.

(C) The fluorescence response of the biosensor and nonresponsive control was tested with the MAPKs ERK2, JNK1α1, JNK2α1, and p38α in the unphosphorylated and phosphorylated state.

(D) Selectivity and specificity of the pE59-C123m87 sensor variant in lysis buffer alone and HEK 293T cell lysate (2 mg/ml total protein) (lysate). The fluorescence response to pERK2 was competed with DARPin EpE82, which binds to the same region of pERK2 as unmodified pE59.

See also Figures S3–S5.

binding specificity previously observed for pE59-wt (Kummer et al., 2012), pE59RFD was highly specific for its cognate target pERK2 and did not interact with any other MAPK or unphosphorylated ERK2 (Figure 2C). Again, the simultaneously assayed sensor-incompetent pE59-ctrl showed no marked response to any tested MAPK either (Figure 2C).

To address applications in living cells, we assessed possible interfering effects from cellular components on the sensor response. pE59RFD selectivity was analyzed by mixing the ERK2 or pERK2 antigen with human embryonic kidney (HEK) 293T cell lysate. The lysate derived from nonstimulated cells resulted in a low level of endogenous pERK2, as confirmed in a previous study (Kummer et al., 2012). The pERK2 sensor selectivity remained remarkably high in the crude lysate and the response range was only slightly diminished compared to buffer samples (Figure 2D). Furthermore, the specificity of the sensor signal was confirmed by a competition experiment using DARPin EpE82, an ERK/pERK binder that had been selected in a previous study (Kummer et al., 2012). DARPin EpE82 binds to the very same region of pERK2 as pE59, but with a considerably higher affinity, and is thus ideally suited for complete inhibition of pE59RFD binding (unpublished data). As expected, the sensor response of pE59RFD was completely abolished in samples containing EpE82 (Figure 2D). We observed only a slight increase of background fluorescence in cell lysate samples with or without EpE82 (Figure 2D, lysate) when compared to cell lysis buffer samples (Figure 2D, black and white bar), indicating an interfering effect from other cellular components. Nonetheless, the dynamic range of pE59RFD remained substantially high.

Modeling of the pERK2-pE59RFD Interface

To understand the molecular mechanism of specificity between the sensor and pERK2, we modeled the pE59-pERK2 complex with the sensor-active dye mero87 and sensor-inactive dye mero53 attached that are chemically similar. We used the crystal structure of pE59-pERK2 (PDB ID code 3ZUV) and applied a step-well energy potential as a constraint to model a covalent bond between C123 and the dye, and between phosphate groups and threonine/tyrosine. We used this model as a starting conformation for discrete molecular dynamics simulations (Dagliyan et al., 2011; Ding et al., 2008; Dokholyan et al., 1998). Based on the number of contacts between the dye and pERK2, mero87 interacts with pERK2 more frequently than mero53, explaining the different fluorescence changes of these two dyes in our experiments (Figures 2A and 3A). Furthermore, interaction energy histograms calculated by MedusaScore (Yin et al., 2008), which measures the interface energy between pERK2 and pE59, revealed an additional population of low-energy conformations of the pE59-C123m87-pERK2 complex relative to the complex of pE59-C123m53-pERK2 (Figure 3B). We also applied a Go-like model (Dagliyan et al., 2011) to pE59-C123m87 to increase the sampling of dye conformations. Based on the obtained representative conformations of pE59-C123m87, the pERK2 activation loop is shifted toward the mero87 docking site (Figure 3C), with the dye positioned along the substrate-binding groove of pERK2 keeping the merocyanine ring system near the pE59-C123m87-pERK2 interface (Figure 3D). All these results suggest that mero87 attachment to C123 is thermodynamically more favorable than the attachment of mero53.

Quantifying the Localized Activation of ERK2 in Live Cells

The pE59RFD biosensor was tested in NIH 3T3 mouse embryo fibroblasts (MEFs) stably expressing YPet, a yellow fluorescent protein derivative (Nguyen and Daugherty, 2005). The introduction of a second fluorophore enabled ratiometric imaging to

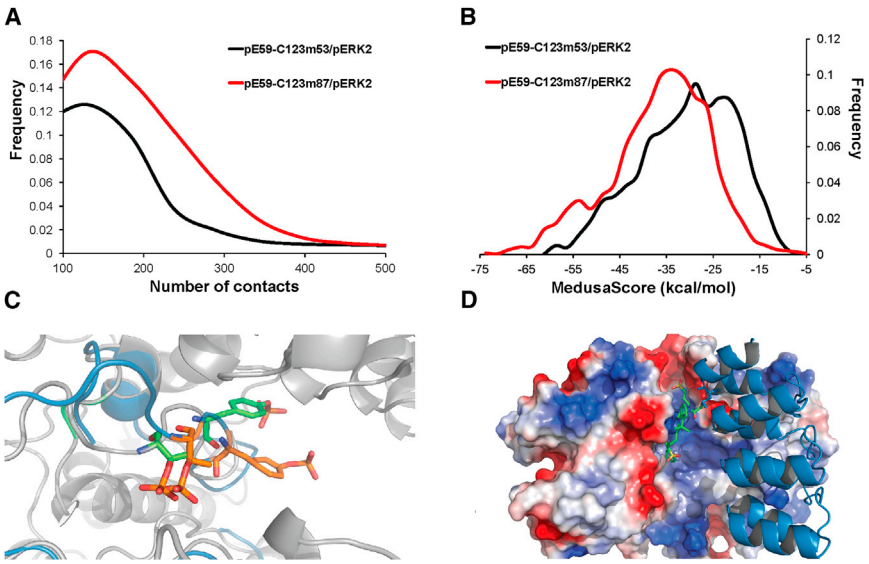

Figure 3. Modeling of pERK2/pE59 with Merocyanine

(A) Distribution of the number of contacts between pERK2 and mero53 (black) and mero87 (red) ($p < 10^{-16}$). This number is defined as distances closer than 5.5 Å between atoms of the dye and the DARPin throughout the trajectories.

(B) Distribution of estimated binding energies (MedusaScore) between pERK2 and pE59 in the presence of mero53 (black) and mero87 (red) dyes ($p < 10^{-16}$).

(C) The activation loop with (orange) and without (green) mero87.

(D) Representative conformation of mero87 docked along with the substrate-binding groove of pERK2.

correct for effects of cell thickness, uneven illumination, and other factors that could affect dye brightness (Bright et al., 1989; Gulyani et al., 2011; Hodgson et al., 2010; Nalbant et al., 2004). ERK activity was indicated by an increase in the dye:YPet emission ratio. The biosensor was loaded into living fibroblasts through microinjection or bead loading and used to map localized ERK activation (Figure 4). The fluorescence ratio showed a nearly 3-fold elevation of ERK activity in the nucleus relative to the cytoplasm, consistent with previous studies of cells in serum (Chen et al., 1992; Gonzalez et al., 1993).

Movies S1 and S2 show the constitutive motility of MEFs. The ERK2 biosensor shows nuclear activation (scaled to maximum to enable visualization of cytoplasmic activation), activity in the perinuclear region, and changing activation in ruffles and membrane protrusions near the cell periphery.

Control studies demonstrated that the observed ERK activation was not due to spurious interactions of the dye with other cellular constituents; the use of a control biosensor with mutations of two crucial contact positions in the DARPin pE59 binding interface (DARPin-pE59 with D46A/R90A), as guided by the pE59-pERK2 complex structure (Kummer et al., 2012), greatly diminished activation (Figure 4). Furthermore, treatment of cells with the ERK pathway inhibitor U0126, which inhibits the upstream kinase MEK1/2 (Favata et al., 1998), also reduced activation (Figure 4), consistent with our other results indicating that the biosensor was specifically reporting ERK activation (Figure 2; Figures S4 and S5).

Surprisingly, even higher activity was observed specifically in nucleoli. This had not been directly observed previously, emphasizing the utility of the biosensor. ERK has been implicated in the induction of rRNA synthesis (Zhao et al., 2003), for which a localization in the nucleolus might indeed be expected.

Because ERK activity is obtained from the ratio of sensor signal over YPet signal, it was important to verify that YPet is not excluded from the nucleolar regions, nor that the DARPin sensor is enriched in the nucleolar regions. It can be seen that the increase in brightness of the DARPin sensor in nucleoli compared to the nuclear region is much stronger (measured as about 2.3-fold by integration of the corresponding areas) than the very slight exclusion of YFP (about 0.85-fold) (Figure S7). To further demonstrate that the increased brightness of the sensor monitors a higher concentration of pERK, and not sensor, in the nucleoli, the background fluorescence was also monitored in the presence of the MEK1/2 inhibitor U0126. No enrichment of the DARPin sensor can be seen (Figure S8). The same is true for the weak-binding DARPin mutant with mutations in the interface (DARPin-pE59 with D46A/R90A) (Figure S9).

In yet another control, mCerulean was directly linked to the DARPin biosensor (Figure S10). In this case, the ratiometric imaging cannot be influenced by any hypothetical different distribution of the sensor and the cell thickness control. This control also demonstrated higher ERK activation in the nucleolus. Because the dye fluorescence was diminished by attachment of mCerulean to the biosensor, we preferred nonetheless to carry out ratio imaging using the separately expressed YPet.

Attempts to study the time course of nuclear ERK activation by growth factors have been unsuccessful so far. Preliminary experiments revealed dynamic activation events in the cytoplasm of motile cells, but these were complex and less intense than the events in the nucleus.

It is possible that the DARPin inhibits nuclear translocation of ERK. Briefly, ERK lacks classical nuclear localization signal sequences (reviewed in Roskoski, 2012). Tyr and Thr phosphorylation in the ERK phosphorylation loop is believed to lead to dissociation from scaffolding proteins, which hold ERK in the cytoplasm. An energy-independent direct transport through interaction with nuclear pore complex proteins appears to involve a region of ERK partially overlapping with the DARPin binding site. Another energy-dependent mechanism engaging residues in the ERK kinase insertion domain, which dock to importin α-7, may also be hindered by DARPin binding.

In vitro kinase assays revealed that pE59-wt sterically inhibits phosphorylation of ERK substrates in a concentration-dependent manner (unpublished data). However, possible effects of RFD biosensors on ERK signaling in living cells were minimized by using the lowest possible biosensor concentrations in vivo. The relatively low affinity of pE59RFD to pERK2 (around 450 nM) is advantageous in this respect, as it leads to weak and transient binding with a fast dissociation phase (Figure S5), favoring detection

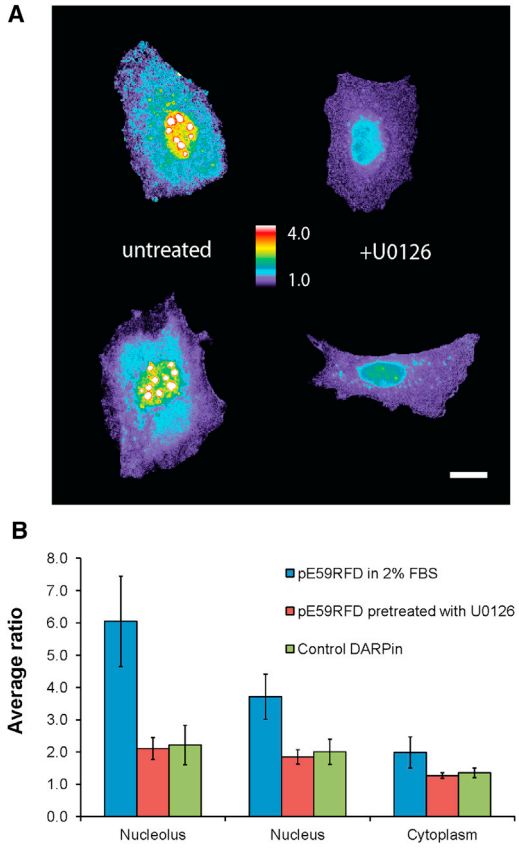

Figure 4. Quantifying Activation of Endogenous ERK in Living Cells

(A) Ratio images of untreated (left) and U0126-pretreated (right) 3T3 mouse embryonic fibroblasts. The scale bar represents 20 μm.

(B) Comparison of the average ratios of the biosensor in 2% fetal bovine serum (blue, 13 cells), pretreated with 10 μM U0126 (red, 46 cells), and the control DARPin in 2% fetal bovine serum (green, 60 cells). Error bars reflect the standard deviation of the average biosensor ratios for the different experimental setups.

See also Figures S6–S10.

rather than inhibition of pERK2 activity. Thus, the design of a DARPin-based biosensor contrasts with that of an inhibitor, for which a high-affinity binding is most effective (Parizek et al., 2012), and DARPins with higher affinity for ERK have been obtained as well (Kummer et al., 2012) but were not chosen for the present study. Nonetheless, we cannot exclude that nuclear localization is inhibited under these conditions, despite having used a DARPin of low affinity and at low concentrations.

The DARPin sensor clearly reacts to the activated kinase in the nucleus. However, the fact that for ERK, unlike for most kinases, nuclear transport is also controlled by residues in the kinase domain makes it more challenging to construct an ERK sensor that interferes with neither activity nor transport. Nonetheless, this work clearly indicates the ability of the biosensor to report dynamics and localization of ERK activation.

DISCUSSION

Fluorescent biosensors can provide new insights into localized activation of proteins in living cells (Welch et al., 2011). Our design of an ERK activity reporter differs significantly from previously reported approaches (Fujioka et al., 2006; Green and Alberola-Ila, 2005; Harvey et al., 2008; Sato et al., 2007). We directly sense the occurrence and localization of endogenous activated ERK by targeting unique features of the active kinase conformation, accounting for sensor specificity. In contrast, fluorescence resonance energy transfer (FRET)-based kinase sensors rely on fluorescence readouts from kinase substrates, which are prone to modification by other cellular enzymes, which thus lead them to report the action of both kinases and phosphatases. Furthermore, activated sensors are subject to diffusion, independent of the actual enzyme target to be monitored. Due to the significantly lower brightness of FRET signals as compared to directly excited dyes, protein dynamics at certain cell positions remain elusive when examined with FRET-based reporters. As an example, Src family kinase activity in protrusion and retraction dynamics was not reported until examined with a dye-labeled monobody biosensor (Gulyani et al., 2011), a design approach similarly aiming for binding to the active enzyme, as in the DARPin-based ERK activity sensor presented here. In the case of ERK, however, the conformational changes upon activation are very subtle, requiring subtractive panning to generate ERK- and pERK-specific binders (Kummer et al., 2012), whose specificity was also studied by X-ray crystallography.

The development of dye-based biosensors derived from natural interaction partners is still hampered by the often tedious optimization of fluorophore attachment for each individual reagent in order to generate appropriate fluorescence readouts. Instead, as proposed recently, biosensors based on affinity reagents, which can be tailored to virtually any target protein of interest, may offer the opportunity to simplify biosensor development by targeting primarily residues near the variable regions for attachment of environmentally sensitive dyes (Brient-Litzler et al., 2010; Gulyani et al., 2011; Miranda et al., 2011). In this regard, the development of binding scaffolds (e.g., DARPins) devoid of cysteines (Binz et al., 2005; Boersma and Plückthun, 2011), thus facilitating site-specific dye attachment, potentially paves the way for a generally applicable approach to biosensor design. If structural data of the complex with the target antigen are available (Brient-Litzler et al., 2010; Kummer et al., 2012), one can easily identify suitable positions for dye conjugation in selected DARPin binders. Yet, even in the absence of any structural information about the interaction interface, the conserved binding mode of designed binding scaffolds enables sensor development. As in the case of DARPins, the target binding site is composed of a number of randomized residues embedded in a constant polypeptide backbone, which guarantees conserved biophysical properties (Binz et al., 2005). In most cases, only a subset of the randomized residues is involved in binding to the target protein. Consequently, suitable positions for dye attachment are either variable positions not involved in binding as determined by site-directed mutagenesis, but located in the neighborhood of the antigen binding site, or are conserved exposed positions adjacent to putative interaction residues (Brient-Litzler et al., 2010; Gulyani et al., 2011; Kummer et al., 2012; Miranda et al., 2011).

In our study, we based the design of an ERK activity sensor on the previously selected DARPin binder pE59 that targets doubly phosphorylated ERK2 selectively both in vitro and in cellular

assays (Kummer et al., 2012) and discriminates against the nonphosphorylated form, which is selectively recognized by DARPin binder E40 (Kummer et al., 2012). The determined structure of the pE59-pERK2 complex facilitated the search for suitable positions to attach solvent-sensitive merocyanine dyes as reporter fluorophores for pERK2 binding. Identified residues for dye coupling were located exclusively at nonvariable framework positions. Remarkably, the replacement of given amino acids by cysteine did not change the conformational integrity of the DARPin scaffold, even though some of them were originally glycines and a destabilizing effect was predicted. This underlines the general robustness of the DARPin framework to carry a mutational load outside the randomized positions without any need for later stability engineering. Therefore, DARPins appear to be a good choice for a generally applicable biosensor scaffold, because the stability of typical library members would allow the incorporation of dyes at a variety of positions, thereby increasing the chances to generate biosensors with desired properties.

Our final ERK activity sensor, pE59RFD, was highly selective for pERK2 in fluorescence assays over ERK2 (Figure 2). No response for other MAPK family members was observed either, highlighting that initial selections of specific DARPin binders can truly yield functional biosensors with the required selectivity and sensitivity. Because of the rather small structural differences that need to be discriminated, it is not surprising that fluorescence properties and binding specificity were dependent on both the positioning and the type of dye used for labeling. As shown exemplarily for DARPin position 123, only conjugation with mero87 resulted in preserved binding behavior and sufficient fluorescence response (Figure 2; Figure S4), as further confirmed by structural modeling (Figure 3). The dye itself thus appears to introduce another element of selectivity.

Importantly for cellular applications, both a high selectivity of binding and a bright fluorescence response are desirable. It is required that nonphosphorylated ERK does not compete with pERK, nor that ERK is sensed. Conversely, affinity to pERK must not be so tight that the sensor acts as a potent inhibitor, and the sensor should not be present in large stoichiometric excess. Although the original DARPin pE59 sterically blocks docking and consequently phosphorylation of F site-containing pERK2 substrates (unpublished data), we used this DARPin specifically because of its moderate affinity combined with high discrimination power. The affinity of pE59RFD for pERK2 (Figure S5) lies in a range proven to be beneficial for biosensor reversibility and specificity (Gulyani et al., 2011; Kraynov et al., 2000; Nalbant et al., 2004; Pertz et al., 2006). In this respect, the 4-fold further decreased affinity of pE59RFD to pERK2, but with retained high discrimination against nonphosphorylated ERK2, in combination with the low sensor concentrations applied here, were useful factors likely minimizing perturbation of ERK signaling in living cells. Nevertheless, it is important to note that essentially all biosensors, including FRET-based sensors, perturb cell physiology to some extent, thus requiring low sensor concentrations and/or controlled experimental conditions to reach meaningful biological conclusions (Gulyani et al., 2011; Harvey et al., 2008).

We used pE59RFD to study ERK activity in living cells (Figure 4), revealing localized activation in the nucleus. This was consistent with previous studies, suggesting that natural ERK signaling functions are not perturbed by pE59RFD: ERK is activated in the nucleus in response to mitogens in serum, with activation persistent as long as the mitogenic stimulus is present (Lenormand et al., 1993). Importantly, the potent inhibitor U0126 of the upstream kinase MEK1/2 (Favata et al., 1998) suppressed activation almost completely (Figure 4). The DARPin-based biosensor revealed ERK activation in the nucleolus, an effect not previously directly observed, but consistent with the involvement of ERK in the induction of rRNA synthesis (Zhao et al., 2003).

SIGNIFICANCE

We have demonstrated that previously determined design principles (Brient-Litzler et al., 2010; Gulyani et al., 2011) are applicable to produce an ERK activity biosensor based on the designed ankyrin repeat protein (DARPin) framework. In the present case, only the altered conformation of the active kinase (Canagarajah et al., 1997; Kummer et al., 2012) is being detected, pointing to a concept applicable to many molecular species undergoing conformational changes in the cell. The conserved binding mode and conformational integrity of alternative binding scaffolds, such as DARPins, potentially simplify sensor design by taking advantage of a generalizable workflow to streamline biosensor production. Combined with dyes of exceptional sensitivity, biosensors may prove to become useful chemical tools in studying subtle changes of protein dynamics in living cells. Due to their favorable biophysical properties and stability, DARPin-based biosensors may also be useful for recent advances in point-of-care immunoassays based on microfluidics (Gervais and Delamarche, 2009) through implementation of both selective capture and sensitive detection of target antigens in one step. Thus, the technology based on long-wavelength solvatochromatic dyes together with DARPins with high discrimination power between conformers holds promise both for in vitro and in vivo applications.

EXPERIMENTAL PROCEDURES

Structural Analysis

The crystal structure of the complex between DARPin pE59 and pERK2 (PDB ID code 3ZUV) (Kummer et al., 2012) was used to calculate solvent-accessible surface areas with the Proteins, Interfaces, Surfaces and Assemblies (PISA) server at the European Bioinformatics Institute (http://www.ebi.ac.uk/pdbe/prot_int/pistart.html) (Krissinel and Henrick, 2007). Contact residues were identified with PISA and the CCP4 software suite (Winn et al., 2011). ΔG values for the folding of DARPin pE59 and its cysteine variants were calculated with ROSETTA (Leaver-Fay et al., 2011).

Molecular Biology

Experiments were performed according to standard protocols (Sambrook and Russell, 2001). Enzymes and buffers were purchased from New England BioLabs or Fermentas. Oligonucleotides were obtained from Microsynth.

Site-Directed Mutagenesis and Cloning

Changes of residues Gly91, Gly113, Asn123, and Gly124 to cysteine as well as Asp46 and Arg90 to alanine in pE59 were made by mutagenesis of plasmid pDST67_pE59 (pE59-wt) (Kummer et al., 2012) using the QuikChange II Site-Directed Mutagenesis Kit (Stratagene). Mutagenic primers (Table S1) were designed as proposed (Brient-Litzler et al., 2010) to avoid primer annealing on nontargeted DNA segments due to the repetitive nature of the DARPin

nucleotide sequence. Mutated DARPin genes were cloned into pDST67 via the BamHI/HindIII sites (Steiner et al., 2008), yielding pDST67_pE59-C91, _pE59-C113, _pE59-C123, _pE59-C124, and _pE59-D46A_R90A (control DARPin).

For a nonresponsive control, we incorporated a cysteine at the N terminus of pE59, a region distant from the interaction interface, to avoid any solvatochromatic effect of attached dyes upon ERK binding. A two-residue insertion, comprising glycine and cysteine, was cloned into pDST67 via EcoRI/BamHI (oligonucleotides pDST67Cf and pDST67r; Table S1). The two residues were inserted behind the N-terminal $MRGSH_6$ tag and directly preceding the BamHI site, which constitutes the 5′ site for DARPin cloning. The modified vector was named pDST67C. The DARPin *pE59* gene was inserted into pDST67C via the BamHI/HindIII sites, yielding pDST67C_pE59 (pE59-ctrl).

Protein Production, Purification, and Characterization

Biotinylated ERK2, pERK2, JNK1α1, pJNK1α1, JNK2α1, pJNK2α1, p38α, and pp38α were produced and purified as outlined previously (Kummer et al., 2012). DARPin pE59-wt and its mutant derivatives, all cloned into pDST67, were expressed and purified as described (Dokholyan et al., 1998). DARPin pE59 cloned into pDST67C was treated accordingly. All DARPins were purified using their hexahistidine tag by IMAC. For cysteine-containing DARPins, buffers were supplemented with 5 mM β-mercaptoethanol throughout the purification process to prevent formation of intermolecular disulfide bonds. IMAC fractions were analyzed by SDS-PAGE. Pure fractions were pooled and stored in sodium phosphate buffer (pH 7.4) supplemented with 150 mM NaCl, 1 mM EDTA, 10% (v/v) glycerol, and 2 mM DTT. Analytical gel filtration was performed in PBS with 2 mM DTT as described (Binz et al., 2003) using purified DARPin variants at 15 μM protein concentration to verify the monomeric state of cysteine-containing DARPins. Binding of DARPin variants to kinases was analyzed by ELISA.

Protein Labeling

The merocyanine dye mero53 has been described previously (Toutchkine et al., 2007b), whereas the dyes mero60, 61, 62, and 87 have been published recently (MacNevin et al., 2013), and mero199 will be described elsewhere (C.M., A. Toutchkine, C.-W. Hsu, L. Li, T.T. Davis, and K.M.H., unpublished data). The storage buffer of pE59 mutants (see above) was exchanged to labeling buffer (sodium phosphate buffer [pH 7.5], 150 mM NaCl, 1 mM EDTA) prior to labeling with dyes using size-exclusion G-25 (GE Healthcare) columns. Thiol-reactive merocyanine dyes (10–20 mM in DMSO) were added to 200 μl DARPins (100–200 μM) in 10-fold excess with less than 10% DMSO in the final reaction mixture. After incubation for 3 hr at room temperature, the reaction was stopped by addition of 1 μl β-mercaptoethanol. The DARPin conjugates were separated from unreacted fluorophore by G-25 size-exclusion chromatography. Labeled proteins were subjected to SDS-PAGE and single fluorescent bands were observed with the molecular weights corresponding to DARPins. Control samples of free dye were visible at lower molecular weight than protein. Labeling efficiencies were calculated by measuring protein and dye concentrations in the purified conjugates. Dye concentrations were estimated using absorbance spectroscopy of the dye at their respective absorption maxima after dissolving the labeled conjugates in DMSO. Protein concentrations were determined with the Pierce 660 nm protein assay (Thermo Scientific) using known concentrations of DARPin pE59 as standards. Binding of labeled conjugates to kinases was analyzed by fluorescence measurements and ELISA.

ELISA

ELISA experiments were performed in PBST (PBS [pH 7.4], 0.05% Tween 20) supplemented with 1 mM DTT. Incubation with detection antibodies was performed in PBST without DTT. Biotinylated ERK2 or biotinylated pERK2 (50 nM each) was immobilized in neutravidin-coated microtiter plates blocked with BSA. Target immobilization and subsequent ELISA steps were performed at 4°C. Purified DARPins or labeled DARPin conjugates (100 nM) were applied to wells with or without immobilized ERK2 antigen for 1 hr. DARPin binding was detected by an anti-RGS-His antibody (1:5,000; QIAGEN), followed by a conjugate of an anti-mouse antibody with alkaline phosphatase (1:10,000; Thermo Scientific). As substrate, *p*-nitrophenylphosphate was used (Sigma).

Fluorescence Measurements

Dye-labeled DARPins (600 nM) in assay buffer (PBS [pH 7.4], 1 mM DTT) were mixed 1:1 (v/v) with target pre-equilibrated in assay buffer (1 μM if not otherwise indicated). Fluorescence spectra were acquired at 25°C using an Infinite M1000 Pro plate reader (Tecan). Excitation was at 595 nm (mero53), 565 nm (mero60), and 585 nm (mero87) for emission spectra. Emission was at 630 nm (mero53), 595 nm (mero60), and 615 nm (mero87) for excitation spectra. One-point measurements were performed with the listed wavelength parameters using a bandwidth of 5 nm for both excitation and emission. Titration of the fluorescence response of the sensor variant pE59-C123m87 and pE59-ctrl was carried out with varying concentrations of ERK2 and pERK2 (final assay concentrations 0.025, 0.05, 0.1, 0.2, 0.4, 0.6, 1.0, 1.5, 3.0 μM).

For assaying the pE59-C123m87 response in cell lysate, HEK 293T cells were lysed in cold lysis buffer (20 mM Tris [pH 7.7], 150 mM NaCl, 0.1 mM EDTA, 2 mM DTT, PhosSTOP phosphatase inhibitor cocktail [Roche], protease inhibitor cocktail EDTA-free [Roche], 1% Triton X-100). The lysate was cleared by centrifugation at 14,000 rpm for 15 min at 4°C. Total protein concentration of the cleared lysate was assessed with the BCA protein assay reagent (Thermo Scientific) using BSA as the standard. For fluorescence measurements, sensor variant pE59-C123m87, ERK target (ERK2 or pERK2), and EpE82 were pre-equilibrated with lysis buffer. The sensor DARPin, ERK antigen, and lysate with or without EpE82 were mixed. For comparison, the same experiment was carried out in lysis buffer without cell lysate. Furthermore, the sensor response in lysate without exogenously added ERK2 was determined. The final protein concentrations in the described lysate assay setups were 300 nM for pE59-C123m87, 300 nM for ERK2, 6 μM for EpE82, and 2 mg/ml (total protein concentration) for the cell lysate.

Surface Plasmon Resonance

SPR was measured using a Biacore 2000 instrument (GE Healthcare). The running buffer was 50 mM Tris (pH 7.4), 150 mM NaCl, 0.05 mM EDTA, and 0.005% Tween 20. Biotinylated ERK2 or pERK2 was immobilized on a streptavidin SA chip (GE Healthcare). Kinetic interaction was measured at a flow rate of 30 μl/min with injection of varying pE59RFD (pE59-C123m87) concentrations followed by an off-rate measurement. The sensorgrams were corrected by subtracting the signal of an uncoated reference cell. Zero-concentration samples (blanks) were included for "double-referencing." The kinetic data were evaluated by fitting the equilibrium binding responses with Scrubber2 (BioLogic Software).

Modeling and Molecular Dynamics of the ERK2-pE59RFD Complex

We mutated Asn123 of pE59 to cysteine using the pE59-pERK2 crystal structure and then attached mero87 and mero53 to this cysteine in silico by applying a step-well potential that mimics a covalent bond (Ding et al., 2008). A similar step-well potential was applied to the phosphate groups on tyrosine and threonine in pERK2. For the investigation of the dynamics of the binding of mero53 and mero87 at the pE59-pERK2 interface, we used discrete molecular dynamics, a well-established efficient molecular dynamics method (Dokholyan et al., 1998) that has been used in different biological applications (Dagliyan et al., 2011; Ding et al., 2010). After the minimization of the system with harmonic constraints at high temperature (0.7 kcal [mol k_B]$^{-1}$) to eliminate steric clashes, the systems were simulated at a temperature of 0.5 kcal (mol k_B)$^{-1}$ for 20 ns. Ten different simulation trajectories (with different initial velocities) for each system were combined and the probability density was calculated based on the number of contacts and MedusaScore (Yin et al., 2008), which is an estimated binding energy that includes van der Waals, solvation, hydrogen bonding, and electrostatic interactions. To measure the significance of two distributions, we calculated p values using the Kolmogorov-Smirnov test. In addition, a simulation with a Go-like model (Dagliyan et al., 2011) -constrained pE59-C123m87 (pE59RFD), where native contacts were kept with another step-well potential to increase the sampling of dye conformations, was performed, and the minimum-energy conformation is represented.

Microscopy

NIH 3T3 MEFs stably expressing YPet, a yellow fluorescent protein variant (Nguyen and Daugherty, 2005), were cultured in 5% CO_2 at 37°C in Dulbecco's modified Eagle's medium (Cellgro) supplemented with 10% fetal calf serum, 2 mM GlutaMAX (GIBCO, Life Technologies), 125 mg/l amphotericin

B (Sigma-Aldrich), and 100 μg/ml penicillin/streptomycin (Cellgro). For imaging experiments, MEFs were plated onto coverslips coated with 5 μg/ml fibronectin (Sigma) overnight. Culture medium was exchanged for imaging medium (Ham's F-12K medium without phenol red [SAFC Biosciences] with 2% fetal bovine serum, 15 mM HEPES, 2 mM GlutaMAX, and 125 mg/l penicillin/streptomycin). The DARPin-based biosensor and the control biosensor were transferred into cells using a bead-loading approach (McNeil and Warder, 1987) or microinjection (Gulyani et al., 2011). Cells were washed twice in PBS and then incubated in 2 ml of imaging medium in 5% CO_2 at 37°C for at least 30 min prior to imaging. For inhibition of ERK signaling, cells were treated with 10 μM U0126 (Sigma).

Imaging was performed on an Olympus IX81 inverted microscope equipped with ZDC focus drift compensator, a cooled digital 14-bit CCD camera (Coolsnap ES-2; Roper Scientific), a 100 W mercury arc lamp, and MetaMorph imaging software (Molecular Devices). Images were acquired using a 40× UPlanFLN 1.3 NA oil immersion objective and processed as described previously (Hodgson et al., 2006). A multiband dichroic mirror (440/505/585, 89006; Chroma) was used with band-pass filters for YPet (ET500/20X and ET535/30M; Chroma), mero87 (HQ572/35X and ET632/60M; Chroma), or mCerulean (ET430/24X and ET470/24M). The average intensities of each image in the cytoplasm, nucleus, or nucleolus were measured using the region statistics function of MetaMorph with manual threshholding. Background, shading correction, and ratio imaging were carried out as previously described (Hodgson et al., 2006). ERK activity was monitored as the ratio of dye:YPet fluorescence (Figure S6). Using intensity thresholding operations (applying a "mask"), the borders of the nucleus and cell edge were identified (Hodgson et al., 2006, 2008).

For comparison of cells, scaling was normalized to be linear between 5% and 95% of maximal activation values.

SUPPLEMENTAL INFORMATION

Supplemental Information includes ten figures, one table, and two movies and can be found with this article online at http://dx.doi.org/10.1016/j.chembiol.2013.04.016.

ACKNOWLEDGMENTS

We thank A. Honegger for calculations of Gibbs free energies of protein variants. L.K. was supported by a doctoral fellowship of the Ernst Schering Foundation. We gratefully acknowledge funding from Schweizerische Nationalfonds grant 3100A0B-128671, the Swiss National Center of Competence in Research in Structural Biology, the PhosphoNetX Project in SystemsX (all to A.P.), the European Union FP7 Collaborative Project AffinityProteome (contract 222635) (to A.P., M.K., and B.Z.), and grant GM090317 from the National Institutes of Health (to K.M.H.). A.P. is a founder and shareholder of Molecular Partners, AG, which commercializes the DARPin technology.

Received: November 13, 2012
Revised: April 11, 2013
Accepted: April 23, 2013
Published: June 20, 2013

REFERENCES

Binz, H.K., Stumpp, M.T., Forrer, P., Amstutz, P., and Plückthun, A. (2003). Designing repeat proteins: well-expressed, soluble and stable proteins from combinatorial libraries of consensus ankyrin repeat proteins. J. Mol. Biol. *332*, 489–503.

Binz, H.K., Amstutz, P., Kohl, A., Stumpp, M.T., Briand, C., Forrer, P., Grütter, M.G., and Plückthun, A. (2004). High-affinity binders selected from designed ankyrin repeat protein libraries. Nat. Biotechnol. *22*, 575–582.

Binz, H.K., Amstutz, P., and Plückthun, A. (2005). Engineering novel binding proteins from nonimmunoglobulin domains. Nat. Biotechnol. *23*, 1257–1268.

Boersma, Y.L., and Plückthun, A. (2011). DARPins and other repeat protein scaffolds: advances in engineering and applications. Curr. Opin. Biotechnol. *22*, 849–857.

Brient-Litzler, E., Plückthun, A., and Bedouelle, H. (2010). Knowledge-based design of reagentless fluorescent biosensors from a designed ankyrin repeat protein. Protein Eng. Des. Sel. *23*, 229–241.

Bright, G.R., Fisher, G.W., Rogowska, J., and Taylor, D.L. (1989). Fluorescence ratio imaging microscopy. Methods Cell Biol. *30*, 157–192.

Canagarajah, B.J., Khokhlatchev, A., Cobb, M.H., and Goldsmith, E.J. (1997). Activation mechanism of the MAP kinase ERK2 by dual phosphorylation. Cell *90*, 859–869.

Chen, R.H., Sarnecki, C., and Blenis, J. (1992). Nuclear localization and regulation of erk- and rsk-encoded protein kinases. Mol. Cell. Biol. *12*, 915–927.

Chen, Z., Gibson, T.B., Robinson, F., Silvestro, L., Pearson, G., Xu, B., Wright, A., Vanderbilt, C., and Cobb, M.H. (2001). MAP kinases. Chem. Rev. *101*, 2449–2476.

Cowley, S., Paterson, H., Kemp, P., and Marshall, C.J. (1994). Activation of MAP kinase kinase is necessary and sufficient for PC12 differentiation and for transformation of NIH 3T3 cells. Cell *77*, 841–852.

Dagliyan, O., Proctor, E.A., D'Auria, K.M., Ding, F., and Dokholyan, N.V. (2011). Structural and dynamic determinants of protein-peptide recognition. Structure *19*, 1837–1845.

Ding, F., Tsao, D., Nie, H., and Dokholyan, N.V. (2008). Ab initio folding of proteins with all-atom discrete molecular dynamics. Structure *16*, 1010–1018.

Ding, F., Yin, S., and Dokholyan, N.V. (2010). Rapid flexible docking using a stochastic rotamer library of ligands. J. Chem. Inf. Model. *50*, 1623–1632.

Dokholyan, N.V., Buldyrev, S.V., Stanley, H.E., and Shakhnovich, E.I. (1998). Discrete molecular dynamics studies of the folding of a protein-like model. Fold. Des. *3*, 577–587.

Favata, M.F., Horiuchi, K.Y., Manos, E.J., Daulerio, A.J., Stradley, D.A., Feeser, W.S., Van Dyk, D.E., Pitts, W.J., Earl, R.A., Hobbs, F., et al. (1998). Identification of a novel inhibitor of mitogen-activated protein kinase kinase. J. Biol. Chem. *273*, 18623–18632.

Fujioka, A., Terai, K., Itoh, R.E., Aoki, K., Nakamura, T., Kuroda, S., Nishida, E., and Matsuda, M. (2006). Dynamics of the Ras/ERK MAPK cascade as monitored by fluorescent probes. J. Biol. Chem. *281*, 8917–8926.

Gervais, L., and Delamarche, E. (2009). Toward one-step point-of-care immunodiagnostics using capillary-driven microfluidics and PDMS substrates. Lab Chip *9*, 3330–3337.

Gonzalez, F.A., Seth, A., Raden, D.L., Bowman, D.S., Fay, F.S., and Davis, R.J. (1993). Serum-induced translocation of mitogen-activated protein kinase to the cell surface ruffling membrane and the nucleus. J. Cell Biol. *122*, 1089–1101.

Green, H.M., and Alberola-Ila, J. (2005). Development of ERK activity sensor, an in vitro, FRET-based sensor of extracellular regulated kinase activity. BMC Chem. Biol. *5*, 1.

Gulyani, A., Vitriol, E., Allen, R., Wu, J., Gremyachinskiy, D., Lewis, S., Dewar, B., Graves, L.M., Kay, B.K., Kuhlman, B., et al. (2011). A biosensor generated via high-throughput screening quantifies cell edge Src dynamics. Nat. Chem. Biol. *7*, 437–444.

Harvey, C.D., Ehrhardt, A.G., Cellurale, C., Zhong, H., Yasuda, R., Davis, R.J., and Svoboda, K. (2008). A genetically encoded fluorescent sensor of ERK activity. Proc. Natl. Acad. Sci. USA *105*, 19264–19269.

Hodgson, L., Nalbant, P., Shen, F., and Hahn, K. (2006). Imaging and photobleach correction of Mero-CBD, sensor of endogenous Cdc42 activation. Methods Enzymol. *406*, 140–156.

Hodgson, L., Pertz, O., and Hahn, K.M. (2008). Design and optimization of genetically encoded fluorescent biosensors: GTPase biosensors. Methods Cell Biol. *85*, 63–81.

Hodgson, L., Shen, F., and Hahn, K. (2010). Biosensors for characterizing the dynamics of Rho family GTPases in living cells. Curr. Protoc. Cell Biol. *46*, 14.11.1–14.11.26.

Kawe, M., Forrer, P., Amstutz, P., and Plückthun, A. (2006). Isolation of intracellular proteinase inhibitors derived from designed ankyrin repeat proteins by genetic screening. J. Biol. Chem. *281*, 40252–40263.

Kraynov, V.S., Chamberlain, C., Bokoch, G.M., Schwartz, M.A., Slabaugh, S., and Hahn, K.M. (2000). Localized Rac activation dynamics visualized in living cells. Science *290*, 333–337.

Krissinel, E., and Henrick, K. (2007). Inference of macromolecular assemblies from crystalline state. J. Mol. Biol. *372*, 774–797.

Kummer, L., Parizek, P., Rube, P., Millgramm, B., Prinz, A., Mittl, P.R., Kaufholz, M., Zimmermann, B., Herberg, F.W., and Plückthun, A. (2012). Structural and functional analysis of phosphorylation-specific binders of the kinase ERK from designed ankyrin repeat protein libraries. Proc. Natl. Acad. Sci. USA *109*, E2248–E2257.

Leaver-Fay, A., Tyka, M., Lewis, S.M., Lange, O.F., Thompson, J., Jacak, R., Kaufman, K., Renfrew, P.D., Smith, C.A., Sheffler, W., et al. (2011). ROSETTA3: an object-oriented software suite for the simulation and design of macromolecules. Methods Enzymol. *487*, 545–574.

Lenormand, P., Sardet, C., Pagès, G., L'Allemain, G., Brunet, A., and Pouysségur, J. (1993). Growth factors induce nuclear translocation of MAP kinases (p42mapk and p44mapk) but not of their activator MAP kinase kinase (p45mapkk) in fibroblasts. J. Cell Biol. *122*, 1079–1088.

MacNevin, C.J., Gremyachinskiy, D., Hsu, C.W., Li, L., Rougie, M., Davis, T.T., and Hahn, K.M. (2013). Environment-sensing merocyanine dyes for live cell imaging applications. Bioconjug. Chem. *24*, 215–223.

Marshall, C.J. (1995). Specificity of receptor tyrosine kinase signaling: transient versus sustained extracellular signal-regulated kinase activation. Cell *80*, 179–185.

McNeil, P.L., and Warder, E. (1987). Glass beads load macromolecules into living cells. J. Cell Sci. *88*, 669–678.

Miranda, F.F., Brient-Litzler, E., Zidane, N., Pecorari, F., and Bedouelle, H. (2011). Reagentless fluorescent biosensors from artificial families of antigen binding proteins. Biosens. Bioelectron. *26*, 4184–4190.

Mosavi, L.K., Cammett, T.J., Desrosiers, D.C., and Peng, Z.Y. (2004). The ankyrin repeat as molecular architecture for protein recognition. Protein Sci. *13*, 1435–1448.

Nalbant, P., Hodgson, L., Kraynov, V., Toutchkine, A., and Hahn, K.M. (2004). Activation of endogenous Cdc42 visualized in living cells. Science *305*, 1615–1619.

Nguyen, A.W., and Daugherty, P.S. (2005). Evolutionary optimization of fluorescent proteins for intracellular FRET. Nat. Biotechnol. *23*, 355–360.

Parizek, P., Kummer, L., Rube, P., Prinz, A., Herberg, F.W., and Plückthun, A. (2012). Designed ankyrin repeat proteins (DARPins) as novel isoform-specific intracellular inhibitors of c-Jun N-terminal kinases. ACS Chem. Biol. *7*, 1356–1366.

Pearson, G., Robinson, F., Beers Gibson, T., Xu, B.E., Karandikar, M., Berman, K., and Cobb, M.H. (2001). Mitogen-activated protein (MAP) kinase pathways: regulation and physiological functions. Endocr. Rev. *22*, 153–183.

Pertz, O., Hodgson, L., Klemke, R.L., and Hahn, K.M. (2006). Spatiotemporal dynamics of RhoA activity in migrating cells. Nature *440*, 1069–1072.

Roskoski, R., Jr. (2012). ERK1/2 MAP kinases: structure, function, and regulation. Pharmacol. Res. *66*, 105–143.

Sambrook, J., and Russell, D.W. (2001). Molecular Cloning: A Laboratory Manual (Cold Spring Harbor, NY: Cold Spring Harbor Laboratory Press).

Sato, M., Kawai, Y., and Umezawa, Y. (2007). Genetically encoded fluorescent indicators to visualize protein phosphorylation by extracellular signal-regulated kinase in single living cells. Anal. Chem. *79*, 2570–2575.

Steiner, D., Forrer, P., and Plückthun, A. (2008). Efficient selection of DARPins with sub-nanomolar affinities using SRP phage display. J. Mol. Biol. *382*, 1211–1227.

Toutchkine, A., Kraynov, V., and Hahn, K. (2003). Solvent-sensitive dyes to report protein conformational changes in living cells. J. Am. Chem. Soc. *125*, 4132–4145.

Toutchkine, A., Nguyen, D.V., and Hahn, K.M. (2007a). Merocyanine dyes with improved photostability. Org. Lett. *9*, 2775–2777.

Toutchkine, A., Nguyen, D.V., and Hahn, K.M. (2007b). Simple one-pot preparation of water-soluble, cysteine-reactive cyanine and merocyanine dyes for biological imaging. Bioconjug. Chem. *18*, 1344–1348.

Welch, C.M., Elliott, H., Danuser, G., and Hahn, K.M. (2011). Imaging the coordination of multiple signalling activities in living cells. Nat. Rev. Mol. Cell Biol. *12*, 749–756.

Winn, M.D., Ballard, C.C., Cowtan, K.D., Dodson, E.J., Emsley, P., Evans, P.R., Keegan, R.M., Krissinel, E.B., Leslie, A.G., McCoy, A., et al. (2011). Overview of the CCP4 suite and current developments. Acta Crystallogr. D Biol. Crystallogr. *67*, 235–242.

Yin, S., Biedermannova, L., Vondrasek, J., and Dokholyan, N.V. (2008). MedusaScore: an accurate force field-based scoring function for virtual drug screening. J. Chem. Inf. Model. *48*, 1656–1662.

Zahnd, C., Pecorari, F., Straumann, N., Wyler, E., and Plückthun, A. (2006). Selection and characterization of Her2 binding-designed ankyrin repeat proteins. J. Biol. Chem. *281*, 35167–35175.

Zhao, J., Yuan, X., Frödin, M., and Grummt, I. (2003). ERK-dependent phosphorylation of the transcription initiation factor TIF-IA is required for RNA polymerase I transcription and cell growth. Mol. Cell *11*, 405–413.

